Punkvang, A., Kamsri, P., Mulholland, A., Spencer, J., Hannongbua, S., & Pungpo, P. (2019). Simulations of Shikimate Dehydrogenase from Mycobacterium tuberculosis in Complex with 3-Dehydroshikimate and NADPH Suggest Strategies for MtbSDH Inhibition. *Journal of Chemical Information and Modeling*, *59*(4), 1422-1433. https://doi.org/10.1021/acs.jcim.8b00834

Simulations of Shikimate Dehydrogenase from *Mycobacterium tuberculosis* in Complex with 3-dehydroshikimate and NADPH Suggest Strategies for *Mtb*SDH inhibition

Auradee Punkvang[a,], Pharit Kamsri[a], Adrian Mulholland[b], James Spencer[c], Supa Hannongbua[d], and Pornpan Pungpo[e]*

[a]Faculty of Science, Nakhon Phanom University, 48000 Nakhon Phanom, Thailand

[b]Centre for Computational Chemistry, School of Chemistry, University of Bristol, Clifton, BS8 1TS Bristol, United Kingdom

[c]School of Cellular and Molecular Medicine, University of Bristol, Bristol BS8 1TD, United Kingdom

[d]Department of Chemistry, Faculty of Science, Kasetsart University, Chatuchak, 10900 Bangkok, Thailand

[e]Department of Chemistry, Faculty of Science, Ubon Ratchathani University, Warinchamrap, 34190 Ubon Ratchathani, Thailand

KEYWORDS: *Mycobacterium tuberculosis*, Shikimate dehydrogenase, shikimate pathway, MD simulation

ABSTRACT

Shikimate dehydrogenase (SDH) from *Mycobacterium tuberculosis* (*Mtb*SDH), encoded by the *aroE* gene, is essential for viability of *M. tuberculosis*, but absent from humans. Therefore, it is a potentially promising target for anti-tuberculosis agent development. Molecular-level understanding of the interactions of *Mtb*SDH with its 3-dehydroshikimate (DHS) substrate and NADPH cofactor will help in the design of novel and effective *Mtb*SDH inhibitors. However, this is limited by the lack of relevant crystal structures for *Mtb*SDH complexes. Here, molecular dynamics (MD) simulations were performed to generate these *Mtb*SDH complexes, investigate interactions of *Mtb*SDH with substrate and cofactor and the role of *Mtb*SDH dynamics within these. The results indicate that, while structural rearrangements are not necessary for DHS binding, reorientation of individual side chains in the NADPH binding pocket is involved in ternary complex formation. The mechanistic roles for Lys69, Asp105 and Ala213 were investigated by generating Lys69Ala, Asp105Asn and Ala213Leu mutants *in silico* and investigating their complexes with DHS and NADPH. Our results show that Lys69 plays a dual role, in positioning NADPH and in catalysis. Asp105 plays a crucial role in positioning both the ε-amino group of Lys69 and nicotinamide ring of NADPH for *Mtb*SDH catalysis, but makes no direct contribution to DHS binding. Ala213 is the selection key for NADPH binding with the nicotinamide ring in the *pro*S, rather than *pro*R, conformation in the *Mtb*SDH complex. Our results identify three strategies for *Mtb*SDH inhibition: prevention of *Mtb*SDH binary and ternary complex formation by blocking DHS and NADPH binding (first and second strategies, respectively); and the prevention of *Mtb*SDH complex formation with either DHS or NADPH by blocking both DHS and NADPH

binding (third strategy). Further, based on this third strategy, we propose guidelines for the rational design of "hybrid" *Mtb*SDH inhibitors able to bind in both the substrate (DHS) and cofactor (NADPH) pockets, providing a new avenue of exploration in the search for anti-TB therapeutics.

INTRODUCTION

Tuberculosis (TB) remains one of the top 10 causes of death worldwide. In 2016, the WHO reported 6.3 million new cases of TB (up from 6.1 million in 2015).[1] New patients with drug-susceptible TB can be cured in six months using the standard regimens, i.e. a combination of first-line TB drugs, including isoniazid, rifampicin, pyrazinamide, ethambutol and streptomycin. However, *Mycobacterium tuberculosis* strains have developed resistance to available TB drugs. Drug-resistant TB is classified as multi drug-resistant tuberculosis (MDR-TB), extensively drug-resistant tuberculosis (XDR-TB) or totally drug-resistant tuberculosis (TDR-TB).[2-4] Due to drug-resistant TB, the standard regimens using existing drugs are now often ineffective. To combat drug-resistant TB, intensive research efforts are being directed towards identification and development of new anti-TB agents. A potential strategy for the development of new drugs against *M. tuberculosis* is to target essential biosynthetic pathways of this bacterium that are absent in humans. This is important to facilitate design of specific anti-TB drugs with low eukaryotic toxicity.

The shikimic acid pathway is present in bacteria, fungi, plants, and in certain apicomplexan parasites, but is absent from humans. Therefore, it is an attractive target for the development of new antimicrobials.[5-8] Seven enzymes involved in this pathway sequentially catalyze a series of chemical reactions for biosynthesis, via shikimate, of chorismate from erythrose 4-phosphate and

phosphoenolpyruvate (Figure 1a).[9] This is a precursor for the biosynthesis of aromatic amino acids, folate and ubiquinone, as well as vitamins E and K.[7,10]

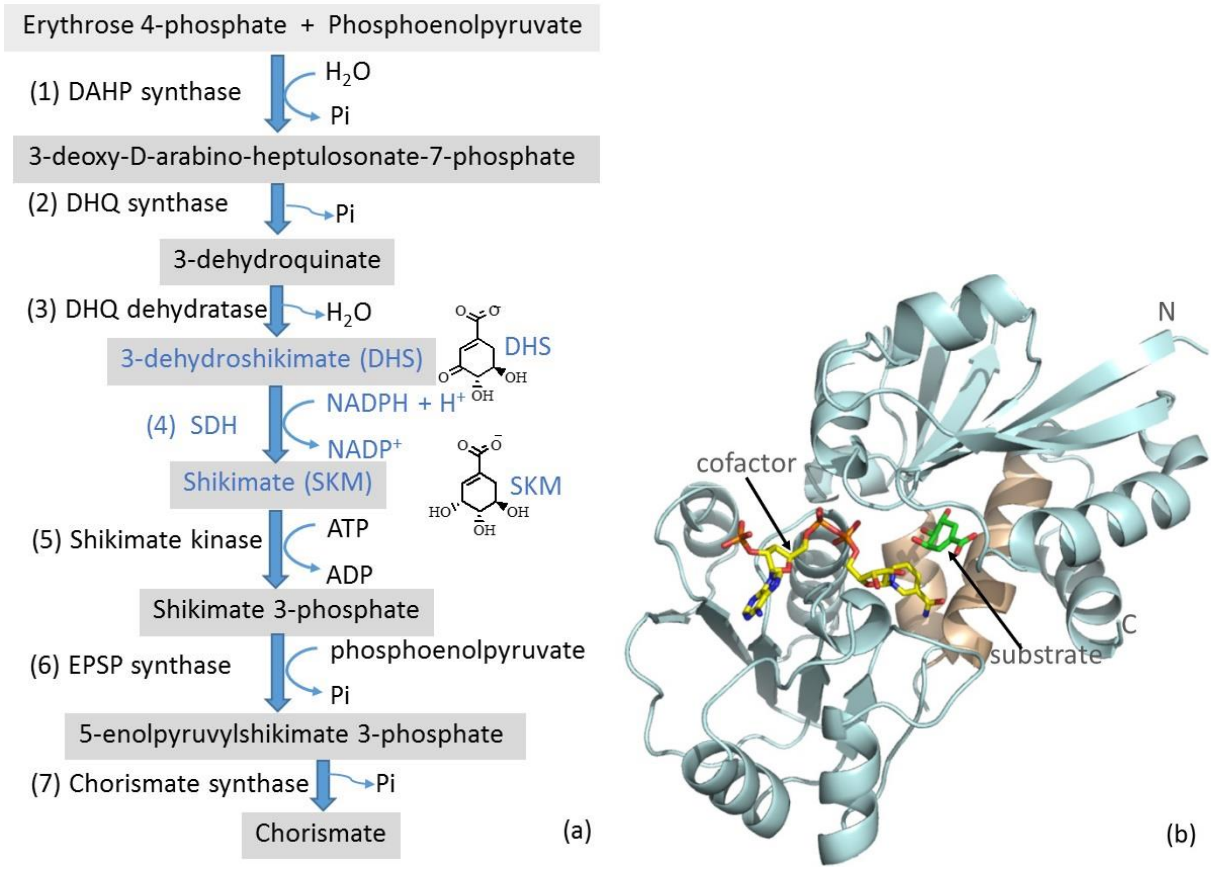

Figure 1. The shikimic acid pathway and Shikimate Dehydrogenase (SDH). **(a)** Shikimate pathway with reactions of the seven enzymes shown. Shikimate dehydrogenase (SDH, the fourth enzyme) is highlighted. **(b)** Structure of SDH (PDB code 3PHI).

Shikimate dehydrogenase (SDH), encoded by the *aroE* gene, participates in the fourth step of the shikimic acid pathway. It catalyzes the reversible, NADPH-dependent, reduction of 3-dehydroshikimate (DHS) to shikimate (SKM) (Figure 1a). The overall structure of SDH (Figure 1b) comprises two α/β domains linked centrally by two α-helices. A deep groove between these two domains contains the active site for the binding of substrate and cofactor.[11-16] The crystal

structures of apo *Mtb*SDH (PDB code 4P4N) and the binary SKM/*Mtb*SDH complex (PDB code 4P4G) have shown that it shares a common three-dimensional structure with all characterized members of the SDH family.[11-16] Kinetic isotope effect and proton inventory studies showed that the kinetic mechanism of *Mtb*SDH follows an ordered bi-bi mechanism. First, DHS binds to the *Mtb*SDH active site to form the binary complex and this is followed by NADPH binding to form the ternary complex (Figure 2a). In the ternary complex, the C4-*pro*S hydride (B side) of NADPH is transferred to DHS in the oxy-reduction reaction of *Mtb*SDH.[17] Interestingly, this differs from the cases of SDH enzymes from *Escherichia coli* (*E. coli* SDH) and *Thermus thermophilus* HB8 (*Tt*SDH), where the C4-*pro*R hydride (A side) of NADPH is instead transferred.[18-19] In the catalytic reaction of *Mtb*SDH, both the hydride transfer from NADPH and the protonation of DHS proceed in the same step, a concerted mechanism (Figure 2b).[17] These experiments also identified that an amino acid residue with an apparent pK_a value of 8.9 participates in the catalytic activity of *Mtb*SDH.[17] Subsequently, site-directed mutagenesis showed that the conserved Lys69 plays a catalytic role: the k_{cat} for wild-type *Mtb*SDH is 68-fold larger than that of the K69A mutant.[20] SDH residues Lys69 and Asp105 (*M. tuberculosis* numbering) are conserved in *Tt*SDH, *E. coli* SDH, *Haemophilus influenzae* SDH, *Arabidopsis thaliana* SDH-like enzyme and *Methanocaldococcus jannaschii* SDH.[17,19] The crystal structures of *Tt*SDH (PDB code 2EV9) and *A. thaliana* SDH-like enzyme (PDB code 2GPT) showed that these invariant residues are coupled by a salt bridge and suggest that these invariant lysine and aspartate residues form a catalytic dyad.[19,21] In the absence of the relevant crystal structures, molecular level information on the binding modes of the DHS substrate and NADPH cofactor to *Mtb*SDH remains lacking. Here, to gain insight into substrate and cofactor binding, binary and ternary *Mtb*SDH complexes were modelled using *in silico* molecular dynamics (MD) simulations. Furthermore, the DHS and NADPH complex structures of

the *Mtb*SDH Lys69Ala (K69A), Asp105Asn (D105N) and Ala213Leu (A213L) mutants were modelled *in silico* to investigate the roles of these residues in *Mtb*SDH mechanism. The findings presented here establish key interactions of substrate and cofactor with *Mtb*SDH and identify mechanistic roles for *Mtb*SDH residues. The results suggest three strategies for *Mtb*SDH inhibition and provide a basis for rational design of hybrid *Mtb*SDH inhibitors interacting with both the substrate and cofactor binding sites.

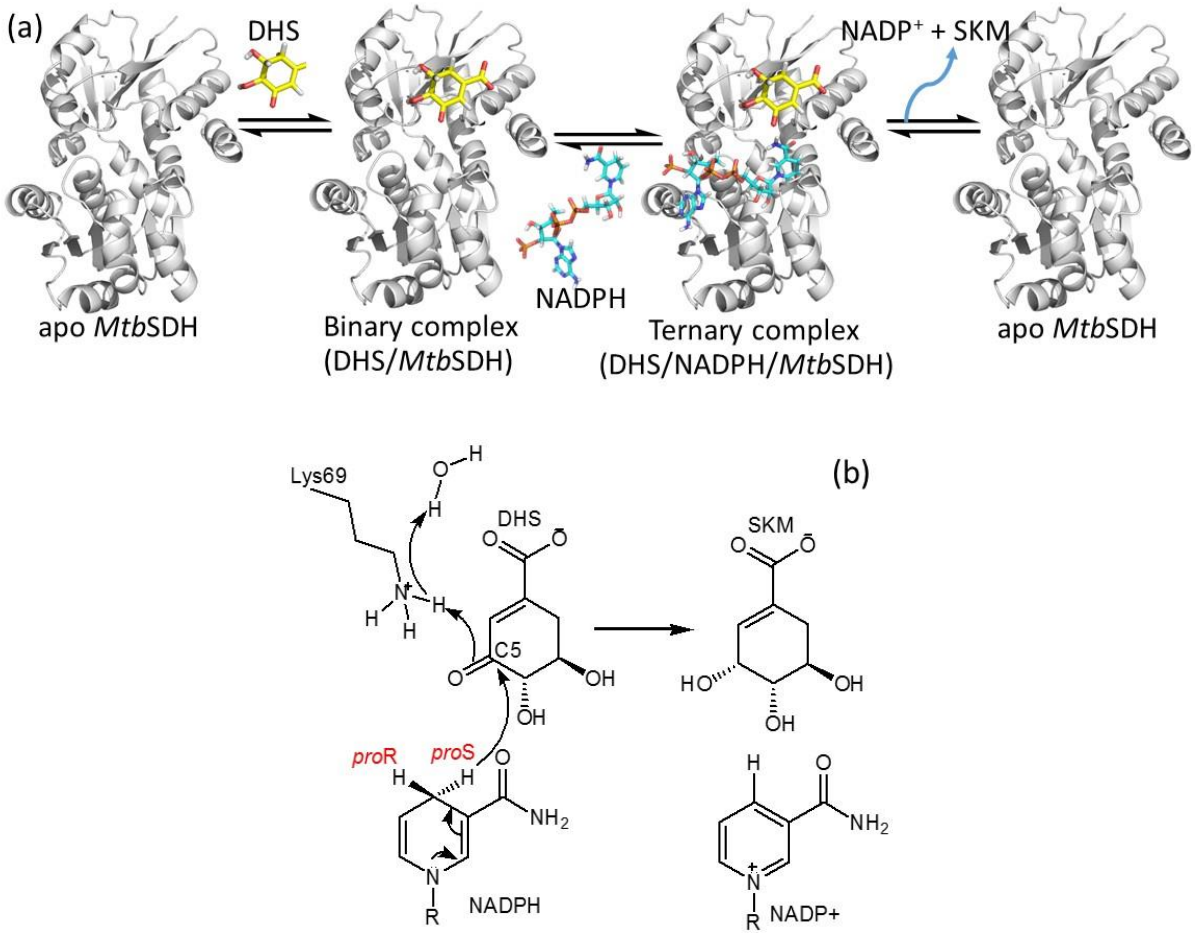

Figure 2. SDH Mechanism. (a) Kinetic mechanism of *Mtb*SDH. Note ordered binding of DHS substrate and NADPH cofactor. **(b)** Proposed concerted catalytic mechanism for *Mtb*SDH.

MATERIALS AND METHODS

Preparation of *Mtb*SDH complex structure

An initial binary DHS/*Mtb*SDH complex structure was generated by molecular docking calculations, as detailed below. Then, it was used to set up a ternary DHS/NADPH/*Mtb*SDH complex structure. The superposition of a binary DHS/*Mtb*SDH complex structure on the x-ray structure of SDH from *Helicobacter pylori* in complex with SKM and NADPH (PDB code 3PHI) was performed to generate the coordinates of NADPH in a ternary DHS/NADPH/*Mtb*SDH complex structure. The nicotinamide ring of NADPH was manually rotated to the *pro*-S conformation, which changed three original torsion angles of O5B-PA-O3-PN, PN-O5D-C5D-C4D and C2D-C1D-N1N-C2N to 147°, -168° and 160°, respectively. A ternary DHS/*pro*R-NADPH/*Mtb*SDH complex structure in which the nicotinamide ring of NADPH is in the *pro*R conformation was prepared similarly to that of the DHS/NADPH/*Mtb*SDH complex, except that the nicotinamide ring of NADPH was not rotated to the *pro*S conformation. The resulting binary and ternary *Mtb*SDH complex structures obtained were used as the initial coordinates for MD simulations and for preparing of mutant enzymes.

Molecular docking calculations

Molecular docking calculations were performed using the Autodock 4.2 program.[22] The coordinates of *Mtb*SDH from the crystal structure of the SKM/*Mtb*SDH complex structure (PDB code 4P4G) were used for these calculations. Forty grid points in the x, y and z dimensions with a grid point spacing of 0.375 Å were used to define the 3D grid box. The grid box was centered on the coordinates of the SKM found in the crystal structure. With exception of the number of GA runs, set to 100, the default search algorithm parameters were employed, including the population

size (150), maximum number of energy evaluations (2,500,000), maximum number of generations (27,000), gene mutation rate (0.02) and crossover rate (0.80). The Kollman and Gasteiger charges were used for *Mtb*SDH and small molecules (SKM and DHS), respectively. Residues of *Mtb*SDH were kept rigid, whereas the structures of SKM and DHS were flexible during the molecular docking calculations. The number of active torsions for SKM and DHS are four and three, respectively. The conformations of small molecules were generated using the Lamarckian Genetic Algorithm (LGA) with 100 GA runs. The RMSD value between the docked and observed x-ray conformations of SKM smaller than 1 Å were used to verify the docking calculations. Then, molecular docking calculations with validated parameters were performed for DHS.

Molecular dynamics simulations

MD simulations were done using AMBER16 software[23] on high performance computing GPU hardware. All missing hydrogen atoms of *Mtb*SDH were added using the LEaP program.[24-25] The Amber ff12SB force field was used for *Mtb*SDH. The general Amber force field (GAFF)[26] and restrained electrostatic potential (RESP) partial charges[27-29] of DHS and NADPH were generated using the Antechamber module implemented in the AMBER16 package. The initial complex structure was solvated with TIP3P water[30] in a truncated octahedral box extending 10 Å from the solute species. Na^+ ions were added to neutralize the system. The total number of atoms in each system for MD simulations was provided in Supporting Information (see Table S1). Energy minimization was performed in two steps, each using a steepest descent algorithm followed by a conjugate gradient algorithm. In the first step, water molecules and counter ions were minimized while restraining all atoms of the solute with a restraint weight of 500 kcal/mol$Å^2$. In the second step, the whole system was minimized with no restraints. Then, the system was gradually warmed from 0 K to 300 K over 30 ps by restraining all atoms of the complex with a restraint weight of 2

kcal/molÅ^2. This was followed by 70 ps of position-restrained dynamics simulation with a restraining weight of 2 kcal/molÅ^2 at 300 K under an isobaric condition. Finally, 150 ns MD simulations for wild-type and mutant *Mtb*SDH systems were performed with no restraints using the same conditions. Three MD simulations of each *Mtb*SDH system were performed to assess the reproducibility of the results. Long-range electrostatic interactions were applied using the particle mesh Ewald (PME) method[31] during the simulations. The cut-off distance for long-range van der Waals interaction was set to 8 Å. The SHAKE method[32] was applied to constrain the bond lengths of hydrogen atoms attached to heteroatoms. Coordinates and energy outputs were recorded every 20 ps during MD simulation. The cpptraj program[33] in AMBER16 was employed to calculate the root mean square deviation (RMSD), root mean square fluctuations (RMSF) and distance between atom pairs of interest. The MM-GBSA interaction energy (see below) was calculated for snapshots collected every 40 ps from the equilibrium state of each system using the python script, MMPBSA.py[34], in the AMBER16 program. The ptraj module in the AMBER12 program[35] was used for hydrogen bond analysis and for cluster analysis of the snapshots collected from the equilibrium state of each system.

Binding free energy calculation

The binding free energy (ΔG_{bind}) of the receptor–ligand complex was estimated from equation 4. The binding free energy (ΔG_{GBSA}) calculated by MM-GBSA approach using the python script (MMPBSA.py[34]) in the AMBER16 program, is the sum of the protein-ligand interaction energy including the electrostatic and van der Waals interaction energies (ΔE_{MM}) and the solvation free energy (ΔG_{sol}) (equation 3). 1250 snapshots extracted every 40 ps from the last 50 ns of 150 ns MD simulations were used for calculation of ΔG_{GBSA}. The $T\Delta S$ term is the entropy contribution to the binding free energy, estimated using normal mode calculation with the python script

(MMPBSA.py[34]) in the AMBER12 program. Because of the high computational cost in the normal mode calculations, 50 snapshots extracted every 1 ns from the last 50 ns of 150 ns MD simulations were used to estimate the entropy contribution.

$$\Delta G_{\text{bind}} = \Delta G_{\text{gas}} + \Delta G_{\text{sol}} \quad (1)$$

$$\Delta G_{\text{gas}} = \Delta E_{\text{MM}} - T\Delta S \quad (2)$$

$$\Delta G_{\text{GBSA}} = \Delta E_{\text{MM}} + \Delta G_{\text{sol}} \quad (3)$$

$$\Delta G_{\text{bind}} = \Delta G_{\text{GBSA}} - T\Delta S \quad (4)$$

RESULTS AND DISCUSSION

1. Stability of MD simulation systems

In the absence of experimental structures, the binary DHS/*Mtb*SDH complex structure, obtained from molecular docking calculations based upon the *Mtb*SDH SKM complex structure (PDB code 4P4G) was used as the initial structure for MD simulations and for preparing binary complexes of two mutant enzymes: *Mtb*SDH (DHS/K69A *Mtb*SDH and DHS/D105N *Mtb*SDH). In the initial structure for MD simulations of the ternary DHS/NADPH/*Mtb*SDH complex, the coordinates of NADPH and DHS were generated by superposition and molecular docking calculations, respectively. The RMSD of DHS, NADPH and *Mtb*SDH with respect to their initial structures was then calculated over the duration of MD simulations to reveal the system stability. Three wild-type systems (apo *Mtb*SDH, binary DHS/*Mtb*SDH and ternary DHS/NADPH/*Mtb*SDH) were equilibrated for ~20 ns, ~50 ns and ~5 ns, respectively, and subsequently remained stable over the rest of the simulation time (150 ns per simulation as described in Methods) for three MD simulations of each system (see Supporting Information

Figure S1). These indicated that wild-type *Mtb*SDH readily reached an equilibrium state when bound to both of DHS substrate and NADPH cofactor. The mutant systems (DHS/K69A *Mtb*SDH, DHS/D105N *Mtb*SDH, DHS/NADPH/K69A *Mtb*SDH and DHS/NADPH/D105N *Mtb*SDH) reached the equilibrium state after ~20 ns, ~50 ns, ~20 ns and ~80 ns, respectively (see Supporting Information Figures S2 and S3). Simulations of ternary complexes of wild-type *Mtb*SDH and the A213L mutant, in which the nicotinamide ring of NADPH is in the *pro*R conformation (DHS/*pro*R-NADPH/*Mtb*SDH and DHS/*pro*R NADPH/A213L *Mtb*SDH, respectively), reached the equilibrium state after ~90 ns and ~40 ns, respectively (see Supporting Information Figure S4). A representative snapshot of the most populated cluster obtained from cluster analysis was selected as the representative structure for each MD simulation (see Supporting Information Table S2). Three representative structures obtained from three MD simulations of each system differed only slightly: across all nine systems tested average RMSD values from pairwise comparisons of replicate simulations were in the range of 1.07-1.44 Å, indicating the reproducibility of the results (see Supporting Information Table S3). Therefore, for each *Mtb*SDH system one of these three representative structures with the highest percent occurrence was selected as the representative structure for that system and used for structural analysis and comparison (see Supporting Information Table S2).

2. Overall structure of *Mtb*SDH

The DHS/NADPH/*Mtb*SDH complex structure modeled here superposes well with the crystal structure of SKM/NADPH/*H. pylori* SDH (Figure 3a). The DHS and SKM substrate found in these structures are positioned in the same pocket and this is observed for NADPH. A deep groove created between N-terminal and C-terminal domains linked centrally by two α-helices is the active site for the binding of DHS substrate and NADPH cofactor (Figure 3b). The binding

residues of DHS and NADPH were defined from DHS/NADPH/*Mtb*SDH complex within the radius of 4 Å from DHS and NADPH. The DHS binding residues are residues 17-20, 63-66, 90 and 247 and those for NADPH are residues 124-129, 149, 153, 191-193, 196, 213, 236, and 239. Residues 69, 105, 215, 240 and 243 participated in binding of both DHS and NADPH. Residues 124-129 form the diphosphate-binding loop which is conserved in the SDH family[19].

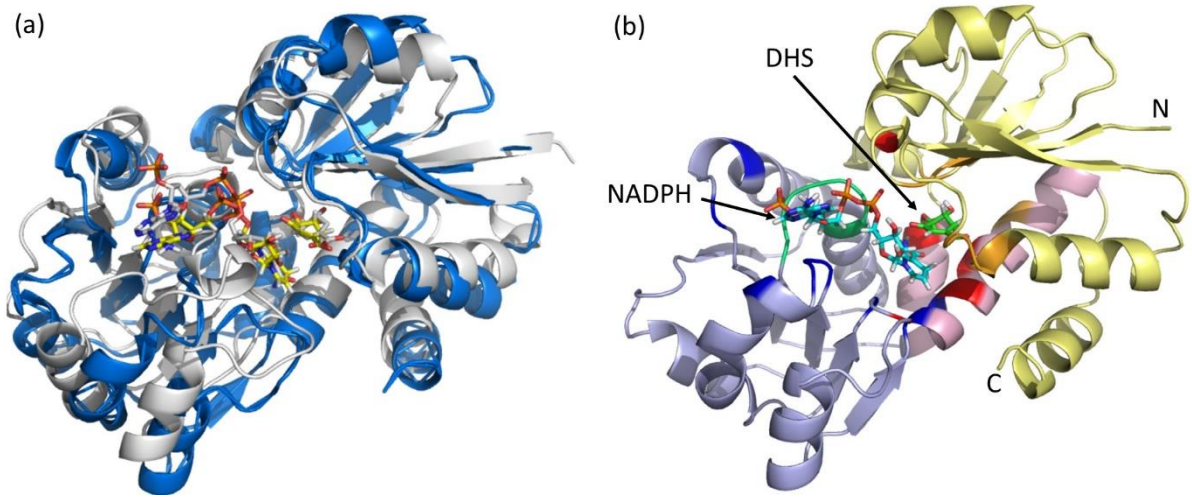

Figure 3. Model of DHS/NADPH/*Mtb*SDH ternary complex. (a) superposition of representative structure of the DHS/NADPH/*Mtb*SDH complex modeled by MD simulation (blue) and the crystal structure of SKM/NADPH/*H. pylori* SDH (PDB code 3PHI, gray). Carbon atoms of DHS/NADPH and SKM/NADPH are colored yellow and gray, respectively. **(b)** DHS/NADPH/*Mtb*SDH ternary complex structure obtained from MD simulations. N-terminal (residues 5-103 and 254-269) and C-terminal (residues 114-235) domains are shown in yellow and purple, respectively. Two α-helical interdomain linkers (residues 104-113 and 236-253) are shown in pink. Colored residues bind DHS (orange), NADPH (blue) or both DHS and NADPH (red); diphosphate-binding loop is colored green.

3. Flexibility of *Mtb*SDH

Successful generation of stable models for *Mtb*SDH and its complexes prompted investigation of enzyme flexibility and the effect upon it of ligand binding and mutation. RMSF values for *Mtb*SDH were calculated from the MD simulations to visualize the flexibility of apo,

ligand-bound and mutant *Mtb*SDHs. RMSF values for ligand-unbound *Mtb*SDH (apo *Mtb*SDH) and ligand-bound *Mtb*SDH (DHS/*Mtb*SDH and DHS/NADPH/*Mtb*SDH) were compared to reveal the influence of ligand binding on the flexibility of *Mtb*SDH. Standard deviations of RMSF values for each *Mtb*SDH residue in these different complexes were calculated to show the difference of their flexibilities. RMSF values of *Mtb*SDH residues in apo *Mtb*SDH, DHS/*Mtb*SDH and DHS/NADPH/*Mtb*SDH were in the range ~2 – 12 Å (Figure S5a). For residues binding either DHS or NADPH as defined above, RMSF values were in the ranges ~2 – 6 Å and ~2 – 7 Å, respectively. The standard deviations of RMSF values for each residue in ligand-unbound and ligand-bound *Mtb*SDHs were in the range ~ 0 – 1 Å (Figure S5a). These data indicate that binding of DHS substrate and NADPH cofactor do not affect the flexibility of *Mtb*SDH. RMSF values of binary complexes of wild-type (DHS/*Mtb*SDH) and mutant (DHS/K69A *Mtb*SDH and DHS/D105N *Mtb*SDH) *Mtb*SDH were then compared to reveal the influence of these mutations on flexibility. RMSF value of *Mtb*SDH residues in these complexes were in the range ~2 – 15 Å (Figure S5b). Standard deviations of RMSF values of each residue in wild-type and mutant *Mtb*SDH were in the range ~ 0 – 3 Å (Figure S5b). This indicates that the K69A and D105N mutations have greater effects on the flexibility of *Mtb*SDH compared to those of ligand binding. However, these mutations showed only a small influence on the flexibility of the DHS and NADPH binding residues, with standard deviation values for these positions in the range ~ 0 – 1 Å (Figure S5b).

4. Structural rearrangement of *Mtb*SDH for DHS and NADPH binding

The conformational change of *Mtb*SDH upon DHS binding was investigated by calculating RMSD values between atoms of apo *Mtb*SDH (PDB code 4P4N) and those of the representative structure for the binary DHS/*Mtb*SDH complex obtained from MD simulations. The backbone

atoms of *Mtb*SDH in the binary DHS/*Mtb*SDH complex superpose well with those of apo *Mtb*SDH as indicated by the small overall RMSD value of 1.35 Å. In the DHS binding pocket, RMSD values of all heavy atoms (backbone and sidechain atoms) of binding residues were in range of 0.5 – 2.5 Å. This indicates that the conformations of the DHS binding residues were not significantly changed upon DHS binding. The exception, His17, had the highest RMSD value (5.2 Å) as His17 changes conformation to interact, *via* a hydrogen bond, with the carboxylate moiety of DHS (Figure 4a). On the other hand, residues Lys69 and Asp105, that are conserved in other SDHs and are coupled by a salt bridge[17,19] showed insignificant positional changes on DHS binding, with small RMSD values of 1.0 and 0.5 Å (Figure 4a), respectively. These data suggest that DHS binding by *Mtb*SDH does not require extensive structural rearrangement. The binding conformation of DHS in the DHS/*Mtb*SDH complex structure obtained after MD simulation was also very similar to that of shikimate (SKM) found in the crystal structure of *Mtb*SDH (PDB code 4P4G; Figure S6). However, compared to the SKM complex, the active site residues significantly rearrange on DHS binding. This rearrangement might result from replacement of the C5 hydroxyl group of SKM with a carbonyl oxygen in DHS. The carbonyl oxygen in DHS moved down as compared to the position of hydroxyl group of SKM. This causes the ε amino group ($-NH_3^+$) of Lys69 moved to the carbonyl oxygen of DHS, inducing repositioning of Asp105 and other residues (Figure S6).

The conformational change of *Mtb*SDH upon NADPH binding was also investigated. Superposition of all backbone atoms in the binary DHS/*Mtb*SDH and ternary DHS/NADPH/*Mtb*SDH complexes obtained from MD simulations showed a small RMSD value of 1.37 Å. In the NADPH binding pocket, RMSD values of all heavy atoms (backbone and sidechain atoms) of NADPH binding residues were in range of 0.5 – 9.9 Å. Residues Lys69 and

Asp105 remained coupled by a salt bridge and showed insignificant positional change on NADPH binding as evidenced by RMSD values of 1.1 Å and 0.5 Å, respectively (Figure 4b). In the diphosphate-binding loop (residues 124-129), there are no large structural changes associated with NADPH binding, as indicated by RMSD values in the range of 1.6 - 3.6 Å. However, two charged residues, Arg149 and Lys153, do undergo significant conformational changes upon NADPH binding, with high RMSD values of 9.9 Å and 6.6 Å, respectively. These large conformational changes of Arg149 and Lys153 are responsible for creating an 'electrostatic clamp'[19] to bind the adenine phosphate of NADPH in the DHS/NADPH/*Mtb*SDH complex (Figure 4b). Thus, *Mtb*SDH requires only specific, highly local, structural rearrangements for NADPH binding. However, NADPH binding does induce positional changes of the DHS substrate and Tyr215 with RMSD values compared to the DHS/*Mtb*SDH binary complex of 2.59 Å and 3.3 Å, respectively. In the ternary complex the DHS substrate lies close to the nicotinamide ring of NADPH and the side chain of Tyr215 interacts with the carboxylate group of DHS (Figure 4b). The remaining residues involved in DHS binding underwent no significant conformational changes on NADPH binding, as indicated by RMSD values in the range of 0.6 - 1.5 Å.

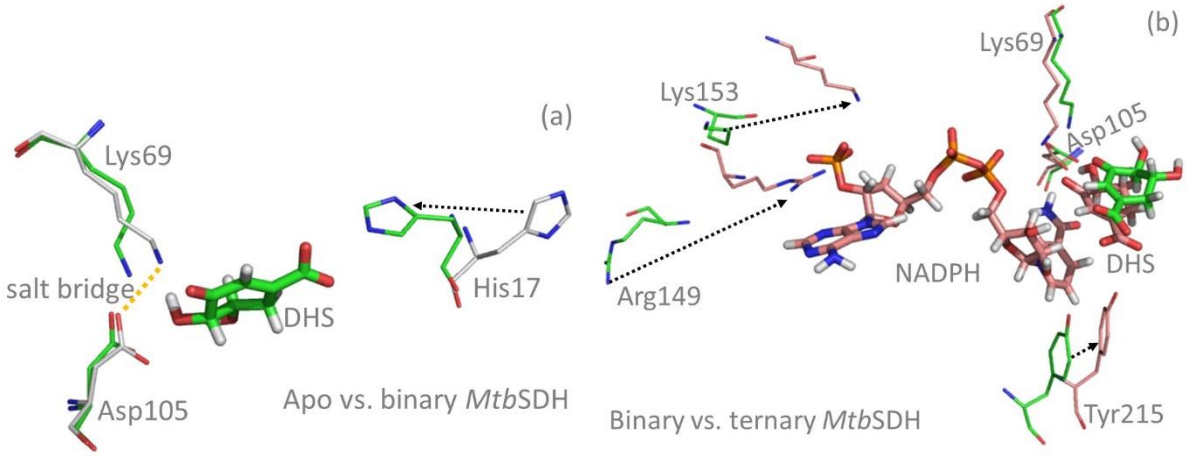

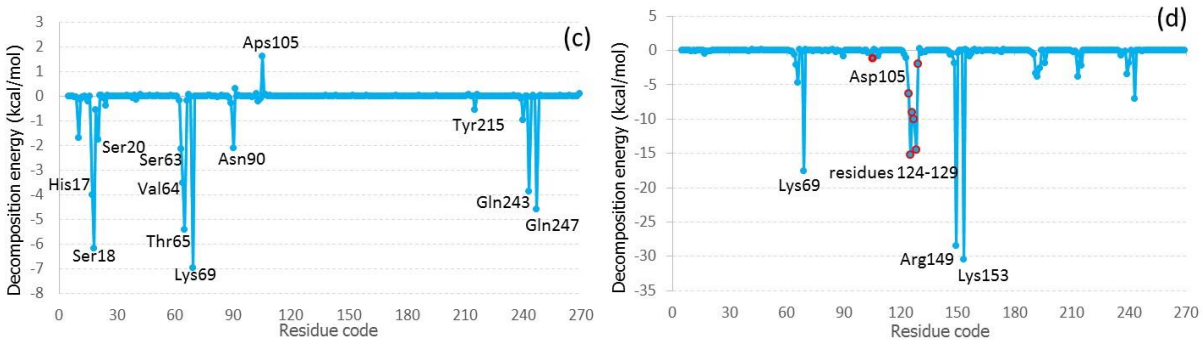

Figure 4. DHS and NADPH binding by *Mtb*SDH. (a) superposition of DHS binding residues in apo *Mtb*SDH (PDB code 4P4N, carbon atoms gray) and binary DHS/*Mtb*SDH complex obtained from MD simulations (carbon atoms green). **(b)** superposition of NADPH binding residues in binary DHS/*Mtb*SDH (carbon atoms green) and ternary DHS/NADPH/*Mtb*SDH (carbon atoms pink) complexes obtained from MD simulations. Black dotted arrows indicate the direction of movement of each residue on NADPH binding. **(c)** and **(d)**, plots of MM-GBSA decomposition energy showing contribution of each *Mtb*SDH residue to DHS binding in the binary DHS/*Mtb*SDH complex and to NADPH binding in the ternary DHS/NADPH/*Mtb*SDH complex, respectively.

5. DHS binding in the binary DHS/*Mtb*SDH complex

In the SKM/*Mtb*SDH crystal structure, SKM forms numerous hydrogen bonds to Ser18, Ser20, Thr65, Lys69, Asn90, Asp105, Tyr215, Gln243 and Gln247. Therefore, hydrogen bond analysis over the equilibrium state of MD simulations was performed for DHS binding in the representative structure for the binary DHS/*Mtb*SDH complex structure. Excepting hydrogen bonds formed by Asn90, Asp105 and Tyr215, all hydrogen bonds involved in SKM binding were retained for DHS binding (Figure S7a). Additional hydrogen bonds to His17, Ser63 and Val64 were formed for DHS binding. The percent occupation of all hydrogen bonds involved in DHS binding (i.e. the number of frames in which each hydrogen bond is considered to form over the

total number of frames selected for hydrogen bond analysis) was in the range of 28 - 100. Notably, hydrogen bonds formed by Ser18, Val64, Lys69, Thr65 and Gln247 showed higher percent occupation (91 - 100) than others. In particular, Ser18 invariably formed a hydrogen bond to DHS (100% occupied) (Figure S7a). The contributions of these hydrogen bonds, as well as other interactions, to DHS binding were further evaluated by their decomposition energies (Figure 4c). The most prominent contributions to DHS binding in *Mtb*SDH, as evidenced by their lower decomposition energies, were made by residues Ser18, Thr65, Lys69, Gln243 and Gln247 forming hydrogen bonds to DHS. These data indicate that hydrogen bonds are the main interaction for DHS binding in *Mtb*SDH. Remarkably, only Asp105 shows a significant positive decomposition energy (~2 kcal/mol) with respect to DHS in the DHS/*Mtb*SDH binary complex (Figure 4c), indicating that this residue makes no contribution to DHS binding in this complex.

6. DHS and NADPH binding in the ternary DHS/NADPH/*Mtb*SDH complex

Models for *Mtb*SDH complexes after MD simulations were next considered with respect to the proposed catalytic mechanism (Figure 2b). Importantly, the positions of DHS and NADPH in the ternary (DHS/NADPH/*Mtb*SDH) complex obtained after MD simulations are consistent with a concerted mechanism. The DHS substrate is located close to the nicotinamide ring of NADPH in the *pro*S conformation (Figure 5a). The trajectory of distance between the *pro*S hydrogen of NADPH and the C5 atom of DHS over 150 ns MD simulations was shown in Figure S8. The average of this distance over the equilibrium state was 4.18 ± 0.40 Å. This is consistent with a *pro*S hydride transfer from NADPH to the C5 atom of DHS in the oxy-reduction reaction catalyzed by *Mtb*SDH (Figure 2b).[17] The NH_3^+ of Lys69 and the C5 carbonyl oxygen of DHS are separated by a distance of 2.86±0.17 Å (Figure 5a), which is consistent with proton transfer

between them. The negatively charged groups of Asp105 and NADPH sandwich the NH_3^+ of Lys69 (Figure 5a), which may serve to facilitate proton transfer.

The electrostatic clamp created by Arg149 and Lys153 interacts with the adenine phosphate of NADPH *via* hydrogen bonds (80-97% occupation) (Figure S7b). This electrostatic clamp showed the highest contribution to NADPH binding in *Mtb*SDH as indicated by the lowest decomposition energy (Figure 4d). The pyrophosphate of NADPH interacts with the diphosphate-binding loop (residues Gly124 - Ala129, forming hydrogen bonds with Ser125, Gly126, Gly127 and Thr128 (Figure S7b). Hydrogen bonds formed by the diphosphate-binding loop are very similar to those found in the $NADP^+$ binding sites of SDH from *E. coli* and *T. thermophilus* HB8 (PDB codes 1NYT and 2EV9, respectively). In addition, Lys69, Asp105 and Gln243 found in the DHS binding pocket formed hydrogen bonds (97-100 % occupied) with NADPH (Figure S7b).

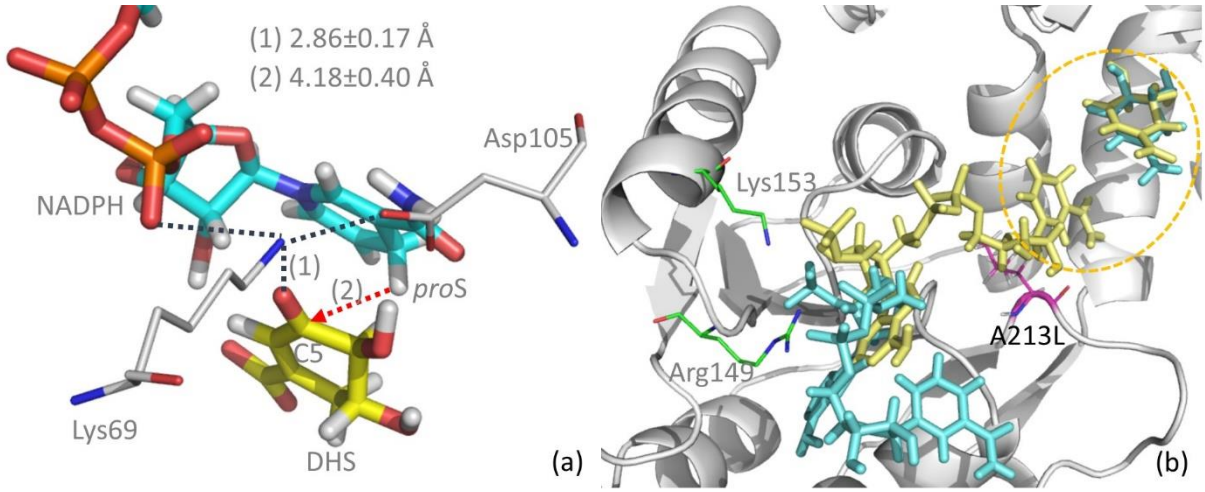

Figure 5. *Mtb*SDH Utilizes NADPH in the *pro*S form. (a) NADPH and DHS binding in representative structure of the ternary DHS/NADPH/*Mtb*SDH complex derived from MD simulations. NADPH and DHS binding shows proposed route of hydride transfer and interactions of Lys69 and Asp105 with NADPH and DHS. Dotted lines indicate interaction, red dotted arrow

indicates the direction of *pro*S hydride transfer. **(b)** binding of NADPH in the *pro*R form to wild-type and A213L *Mtb*SDH. NADPH and DHS binding in representative structures of the DHS/*pro*R-NADPH/*Mtb*SDH (cyan) and DHS/*pro*R NADPH/**A213L** *Mtb*SDH (yellow) ternary complexes. The catalytic pocket, electrostatic clamp (Arg149 and Lys153) and site of the Ala213Leu mutation are highlighted in orange dotted circle, green and pink, respectively.

7. Selection of *pro*S conformation of NADPH nicotinamide ring

The oxy-reduction reaction of *Mtb*SDH occurs by transfer of the C4-*pro*S hydride (B face) of NADPH to DHS (Figure 2b).[17] This differs from the cases of SDH enzymes from *H. pylori*, *E. coli* and *Tt*SDH, where the C4-*pro*R hydride (A face) of NADPH is instead transferred.[18-19] Hence MD simulations of a ternary DHS/NADPH/*Mtb*SDH complex structure in which the nicotinamide ring of NADPH is in the *pro*R conformation (DHS/*pro*R-NADPH/*Mtb*SDH) were undertaken to investigate why *pro*R hydride transfer is not favored for *Mtb*SDH. 150 ns MD simulations of the DHS/*pro*R-NADPH/*Mtb*SDH ternary complex showed that in the *pro*R conformation the nicotinamide ring of NADPH did not remain in the catalytic pocket of *Mtb*SDH, responsible for binding the DHS substrate and NADPH nicotinamide ring, although NADPH remained bound to *Mtb*SDH due to retention of interactions with the electrostatic clamp (Figure 5b). These data indicate that *Mtb*SDH is unable to bind NADPH in the *pro*R conformation in an orientation competent for hydride transfer.

To further investigate why *Mtb*SDH does not favor binding of the nicotinamide ring of NADPH in the *pro*R conformation, the respective NADPH binding pockets for *Mtb*SDH and *H. pylori* SDH were compared (Figure S9). The conformations of Lys69, Gly236, Met239 (*Mtb*SDH numbering) in both enzymes are similar. In *H. pylori* SDH, the *pro*R nicotinamide ring of NADPH

forms a hydrogen bond to the invariant glycine (Gly230) and interacts with the two hydrophobic sidechains of Leu208 and Met233. However, in *Mtb*SDH the smaller sidechain of Ala213 replaces the alkyl hydrophobic sidechain of Leu208 in *H. pylori* SDH, suggesting that the differing sidechains of Leu208 and Ala213 respectively select for the *pro*R and *pro*S forms of the NADPH nicotinamide ring. To test this hypothesis, MD simulations of a ternary DHS/*pro*R-NADPH/*Mtb*SDH structure containing the Ala213Leu (A213L) mutant (DHS/*pro*R NADPH/A213L *Mtb*SDH) were performed. MD simulations showed that *pro*R NADPH in the A213L mutant complex readily reached an equilibrium state (~5 ns), whereas this in the wild-type complex difficultly reached an equilibrium state (~90 ns), (see Supporting Information Figure S4). In contrast to the wild-type enzyme, the *pro*R nicotinamide ring of NADPH remains bound in the catalytic pocket of the A213L *Mtb*SDH mutant (Figure 5b). Accordingly, we conclude that in *Mtb*SDH the sidechain of Ala213 selects for the *pro*S form of the NADPH nicotinamide ring toward to the *pro*S hydride transfer favoured for *Mtb*SDH.

8. Roles of Lys69 and Asp105 in the reaction of *Mtb*SDH

The role of Lys69 in the catalytic mechanism of *Mtb*SDH has been investigated experimentally. Steady-state kinetic measurements showed that the turnover number (k_{cat}) for wild-type *Mtb*SDH (50 s^{-1}) is 68-fold greater than that for the K69A mutant (0.73 s^{-1}), indicating a critical role in catalysis for Lys69, probably in proton transfer to the C5 carbonyl of DHS.[20] In *Mtb*SDH Lys69 and Asp105 are coupled by a salt bridge (Figure 6a), suggesting that Asp105 may also have a mechanistic function, possibly by affecting either the flexibility of Lys69 or the distance between Lys69 and DHS during the catalytic reaction. Therefore, we modelled the D105N mutant in complex with DHS (DHS/D105N *Mtb*SDH complex) to investigate the role of Asp105 in the catalytic function of *Mtb*SDH. Specifically, the distance between the C5 carbonyl oxygen

atom of DHS and the ε amino nitrogen atom (-NH_3^+) of Lys69 was measured over the equilibrium state of MD simulations for DHS/*Mtb*SDH and DHS/D105N *Mtb*SDH binary complexes (Note that, as described above, the mutation exerted only limited effects on the global dynamics of *Mtb*SDH). In the simulation of the DHS/*Mtb*SDH complex, the average distance between the DHS C5 carbonyl oxygen and the Lys69 ε amino nitrogen atom was 2.89±0.34 Å (Figure 6a), close to that observed (2.94 Å) for the Lys69 ε amino nitrogen and the C5 hydroxyl oxygen of SKM in the crystal structure of the SKM/*Mtb*SDH complex (PDB 4P4G). For the D105N mutant this average distance was 5.22±2.06 Å (Figure 6b), almost double that found in wild-type *Mtb*SDH, indicating that proton transfer to C5 is hampered in the D105N mutant *Mtb*SDH. Moreover, the ε amino nitrogen atom of Lys69 in the D105N mutant *Mtb*SDH was much more mobile than in wild-type *Mtb*SDH (Figures 6a and 6b). Accordingly, our simulations suggest that Asp105 plays a crucial rule in fixing the ε-amino group of Lys69, via a salt bridge, in a suitable position to participate in the catalytic reaction of *Mtb*SDH. In support of this conclusion, the D423N mutant of the *A. thaliana* SDH-like enzyme, (equivalent to the D105N mutant of *Mtb*SDH), showed substantial reduction in k_{cat} values from 428 s^{-1} (wild-type) to 0.121 s^{-1}, (D423N mutant).[21] Thus mutation of Asp105 would be expected to decrease the catalytic activity of *Mtb*SDH.

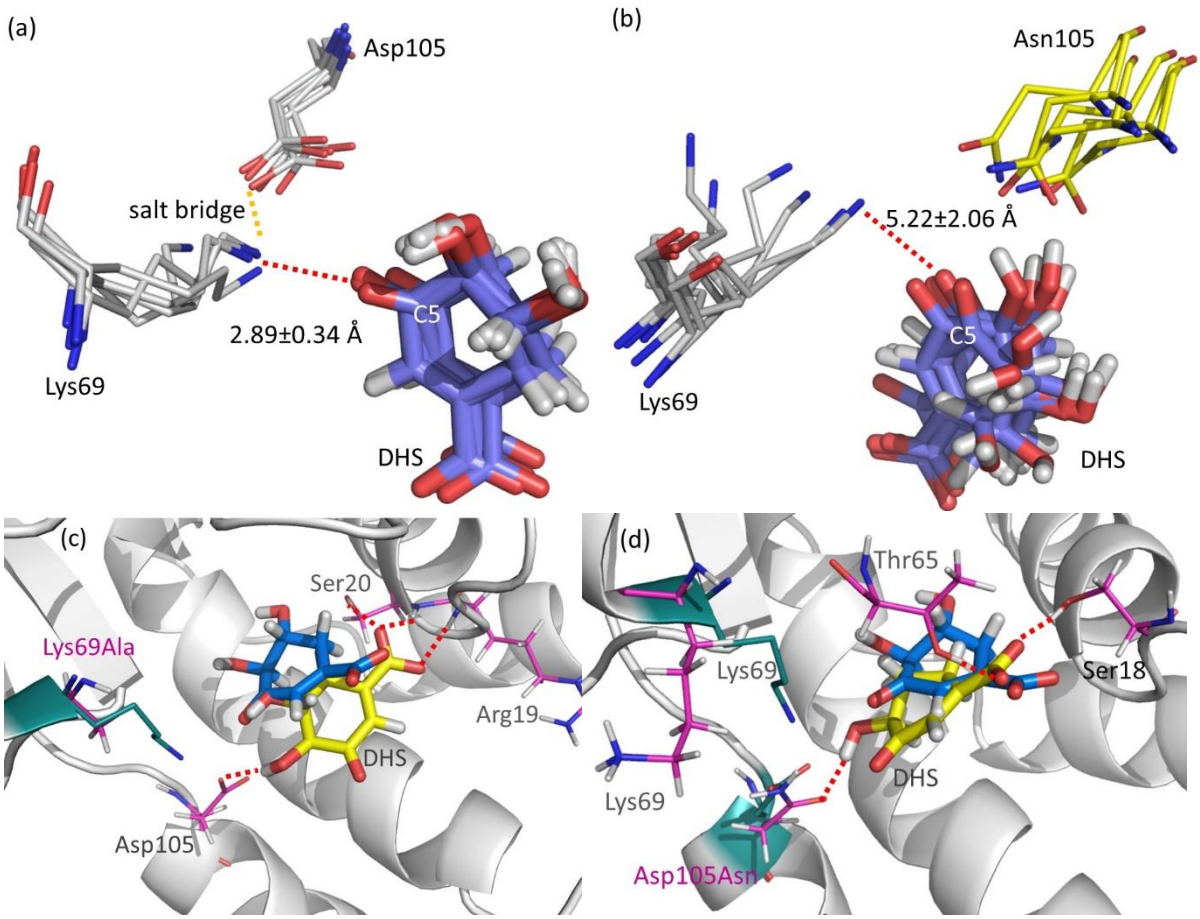

Figure 6. Effects of mutations at *Mtb*SDH Lys69 and Asp105. Motion of Lys69 in **(a)** wild-type and **(b**) D105N *Mtb*SDH. Figure shows distances between the DHS C5 carbonyl oxygen and Lys69 ε amino nitrogen atom averaged over the equilibrium state of each simulations for representative structures generated by cluster analysis after MD simulations of DHS complexes. **(c)** Effect of K69A and **(d)** effect of D105N mutations on DHS binding. Superpositions of DHS in representative structures obtained after MD simulations for wild-type (DHS carbon atoms blue) and mutant (DHS carbon atoms yellow) *Mtb*SDH binary complexes. Carbon atoms of identified residues in wild-type and mutant *Mtb*SDH are green and pink, respectively. Red dotted lines indicate hydrogen bonds formed by *Mtb*SDH mutants.

9. Roles of Lys69 and Asp105 in DHS and NADPH binding by *Mtb*SDH

In the binary complex of DHS and *Mtb*SDH, Lys69 showed stronger interaction energies than other residues (Figure 4c), indicating a greater contribution to DHS binding. Moreover, it formed persistent hydrogen bonds to DHS, with 92% occupancies over the equilibrium state of MD simulations (Figure S7a). However, experiments indicate that Lys69 plays only a minor role in DHS binding, as evidenced by comparison of K_M values for DHS in wild-type and K69A mutant *Mtb*SDH of 29 and 76 μM, respectively.[20] Similarly, Asp105 showed a positive decomposition energy (~2 kcal/mol) for DHS binding in the binary *Mtb*SDH complex, and did not form hydrogen bonds with DHS (Figures 4c and S7a). In the *A. thaliana* SDH-like enzyme, mutation of Asp423, equivalent to Asp105 in *Mtb*SDH, to Asn (D423N) does not affect the binding affinity for shikimate as indicated by K_M values for wild-type enzyme and the D423N mutant of 685 and 555 μM, respectively.[21] Given the apparent discrepancy between these data and the results of our decomposition analysis, we sought to investigate the possible role of residues 69 and 105 in DHS binding using MD simulations of binary DHS complexes of K69A and D105N *Mtb*SDH (DHS/K69A *Mtb*SDH and DHS/D105N *Mtb*SDH, respectively). Our results showed that the K69A and D105N mutants did not significantly change the binding free energies of DHS in *Mtb*SDH, as evidenced by the calculated binding free energies for DHS in wild-type, K69A and D105N mutant *Mtb*SDH (-33.6, -29.5 and -34.3 kcal/mol, respectively, Table 1).

However, the K69A mutation significantly changes the binding position of DHS as compared to that in wild-type *Mtb*SDH (Figure 6c). The carboxylate group of DHS moves closer to Arg19 and Ser20, resulting in formation of three hydrogen bonds and an additional interaction with Ser18. These interactions showed negative decomposition energies in the range ~4-6 kcal/mol, lower than other residues (~0-2 kcal/mol) (see Supporting Information Figures S10a).

Furthermore, the DHS C4 hydroxyl group is held in place by a hydrogen bond to Asp105 (Figure 6c) with a negative decomposition energy ~2 kcal/mol. Remarkably, Asp105 shows a significant positive decomposition energy (~2 kcal/mol) with respect to DHS binding to wild-type *Mtb*SDH (Figure 4c). These results indicate that Asp105 contributes to DHS binding in the *Mtb*SDH K69A mutant. Thus, additional hydrogen bonds formed between DHS, Arg19, Ser20 and Asp105 in K69A *Mtb*SDH may compensate for the loss of interactions involving Lys69 in the wild-type enzyme, and may help to maintain k_M values for DHS at the same level.

In D105N *Mtb*SDH, the binding position of DHS changes only slightly as compared to that in the wild-type enzyme (Figure 6d), and the decomposition energy patterns of DHS binding in wild-type and mutant D105N *Mtb*SDH are similar (Figures 4c and S10b, respectively). The most prominent contributions to DHS binding in D105N *Mtb*SDH, involve hydrogen bonds formed by residues Ser18 and Thr65, as evidenced by their lower negative decomposition energies (~5 kcal/mol). Further, DHS formed an additional hydrogen bond to the mutated residue Asn105, also with a negative decomposition energy (~3 kcal/mol). These additional interactions compensate for the loss of the salt bridge created between Lys69 and Asp105 in wild-type *Mtb*SDH (see above) with consequent loss of a hydrogen bond between DHS and Lys69. Our analysis however indicates that, consistent with experimental data from the *A. thalania* system, in wild-type *Mtb*SDH, Asp105 makes no direct contribution to DHS binding.

Table 1. The calculated binding free energies (ΔG_{bind}) of DHS in wild-type, K69A and D105N mutant *Mtb*SDH complexes (DHS/*Mtb*SDH, DHS/K69A *Mtb*SDH, DHS/D105N *Mtb*SDH).

System	[a]ΔG_{GBSA}	$-T\Delta S$[a]	[a]ΔG_{bind}
DHS/*Mtb*SDH	–18.4±3.9[b]	–15.2±2.2 [b]	–33.6±2.7 [b]
DHS/K69A *Mtb*SDH	–13.4±5.3	–16.1±1.1	–29.5±6.3
DHS/D105N *Mtb*SDH	–17.3±3.7	–17.0±0.7	–34.3±3.7

[a]The value was averaged from three MD simulations of each complex.
[b]The standard deviation value (sd) of each term obtained from three MD simulations.

Decomposition analysis of interaction energies for NADPH binding in the ternary DHS/NADPH/*Mtb*SDH complex (see above) identifies the electrostatic clamp created by Arg149 and Lys153 as making the greatest contribution to NADPH binding by *Mtb*SDH (Figure 4d), consistent with investigations of SDHs from *E. coli* and *T. thermophilus* HB8 that support a crucial role for the electrostatic clamp in binding the adenine phosphate of NADP. [13,19] However, after the electrostatic clamp, Lys69 shows the lowest decomposition energy for NADPH binding, and forms a hydrogen bond to NADPH at 97% occupation over the equilibrium state of MD simulations (Figures 4d and S7b). Furthermore, although Asp105 showed a positive decomposition energy (~2 kcal/mol) for DHS binding in the binary complex (Figure 4c), it had a negative decomposition energy (~1 kcal/mol) for NADPH binding in the ternary complex (Figure 4d) and formed a hydrogen bond (98% occupation) with NADPH (Figure S7b). Thus, both Lys69 and Asp105 may be important in NADPH binding by *Mtb*SDH. Accordingly, ternary complexes of the K69A and D105N mutants (DHS/NADPH/K69A and DHS/NADPH/D105N *Mtb*SDH) were simulated in order to investigate the roles of these residues in NADPH binding. For both mutations, NADPH remained bound in simulations of the respective ternary (DHS/NADPH/*Mtb*SDH) complexes, but, compared to the wild-type complex, in neither case was the *pro*S nicotinamide ring of NADPH located in a suitable position to participate in the catalytic reaction (Figure 7) and in both mutants

NADPH is more mobile than in the wild-type enzyme (see Supporting Information Figures S3 and S1c, respectively). Our simulations show that both Lys69 and Asp105 have dual roles in *Mtb*SDH, being involved in the catalytic reaction and in positioning the *pro*S nicotinamide ring of NADPH for catalysis.

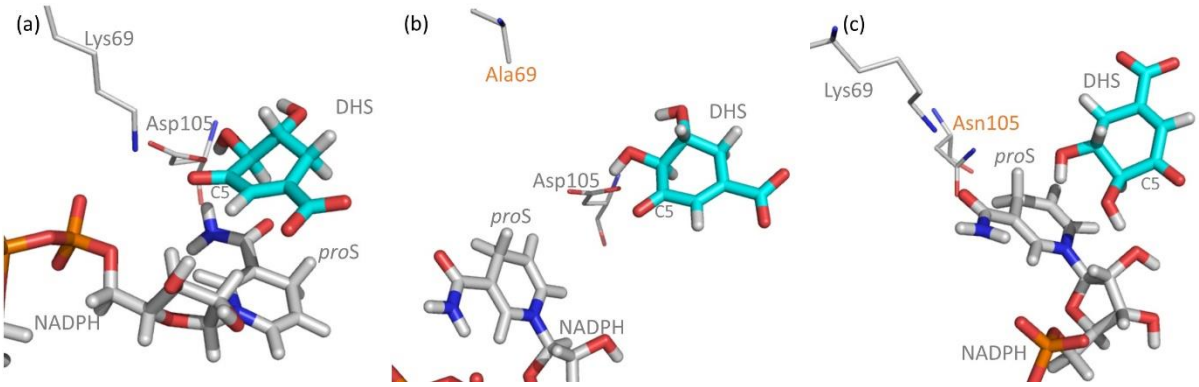

Figure 7. NADPH and DHS binding to ternary *Mtb*SDH complexes. Models of **(a)** wild-type, **(b)** K69A and **(c)** D105N *Mtb*SDH ternary complexes. Models shown are representative structures obtained after MD simulations as described above. DHS carbon atoms are shown in cyan; NADPH carbons in gray.

DISCUSSION

Strategy for *Mtb*SDH inhibition

Binary and ternary complexes of *Mtb*SDH with DHS substrate and NADPH cofactor modelled here by MD simulations provide molecular-level understanding of the interactions and structural rearrangement of *Mtb*SDH for binding its substrate and cofactor. Combining information from these models of the *Mtb*SDH complexes with proposed catalytic mechanisms of *Mtb*SDH allows us to propose three possible strategies for *Mtb*SDH inhibition by small molecules. The first strategy is prevention of binary complex formation in the first step of *Mtb*SDH catalysis (Figure 2a) by competitive inhibition by small molecules with respect to the DHS substrate, i.e. DHS-

competitive inhibitors that resemble the substrate and bind to the DHS binding pocket. The DHS binding pocket does not require structural rearrangement for substrate binding, as evidenced by comparison of RMSD values for simulations of apo and DHS-bound *Mtb*SDH. Therefore, the size and shape of DHS-competitive inhibitors should mimic those of the DHS substrate. Further, our decomposition analysis shows that Lys69 and Ser18 make the largest contributions to DHS binding, forming hydrogen bonds to the DHS C5 carbonyl and carboxylate oxygen atoms, respectively. Small molecules able to form hydrogen bonds with these residues would thus be promising DHS-competitive inhibitors.

The second inhibition strategy is blocking of NADPH binding in the second step of *Mtb*SDH catalysis (Figure 2a), i.e. preventing formation of the *Mtb*SDH ternary complex. Our simulations show that in *Mtb*SDH the electrostatic clamp created by Arg149 and Lys153 shows the strongest interaction for NADPH binding with high negative decomposition energies (~30 kcal/mol) (Figure 4d). However, Arg149 and Lys153 require specific structural rearrangements to create the electrostatic clamp, as detailed in the previous section, making it difficult for small molecules to bind competitively in this site. Alternatively, small molecules able to bind in the binding pocket of the nicotinamide ring of NADPH might present a more promising strategy. In this pocket, the NADPH *pro*S nicotinamide ring forms hydrogen bonds to Asp105, Thr128 and Gln243 with % occupations in the range of 73 – 100% (Figure S7b). Moreover, this moiety interacts with the hydrophobic side chain of Ala213, proposed here to be important as the basis for selection of the *pro*S conformation of the nicotinamide ring, as well as with the hydrophobic side chains of Thr128, Thr191 and Met239 (Figure 8a). Therefore, small molecules bearing both hydrophobic and hydrophilic moieties, thus enabling hydrophobic interactions with Thr128, Thr191, Ala213 and Met239 and hydrogen bonds to Asp105, Thr128 and Gln243, would be

expected to bind in the nicotinamide ring binding pocket and act competitively with respect to NADPH.

A final strategy for *Mtb*SDH inhibition is the prevention of both DHS and NADPH binding. Small molecules utilising the binding pockets for both DHS and the NADPH nicotinamide ring would be required to implement this strategy, and would be expected to act as competitive inhibitors with respect to both DHS substrate and NADPH cofactor. A combination of structural features of small molecules identified using the first and second strategies would be required for this type of competitive inhibitor. In other systems, approaches targeting two substrate-binding sites of a single enzyme successfully identified an inhibitor with low nanomolar potency.[36] Therefore, we propose *Mtb*SDH inhibitors targeting the binding pockets of both DHS and of the *pro*S nicotinamide ring of NADPH and term these hybrid inhibitors (Figure 8b). Head and tail groups would follow those of compounds identified using the first and second inhibition strategies, with the tail of the hybrid inhibitor attached to the head group via a linker equivalently positioned to a location between the C5 carbonyl and carboxylate oxygen atoms of DHS, in order to facilitate binding in the nicotinamide ring pocket (Figure 8b). Furthermore, as hydrophilic agents only slowly cross the mycobacterial cell wall,[37] hydrophilic moieties in the tail would be removed in order to balance the hydrophilicity of hybrid inhibitors arising from the likely presence of negatively charged carboxylate groups at the head. As growing evidence indicates that presence of negatively charged carboxylate groups on small molecule compounds decreases activity against *M. tuberculosis*,[39] our preferred strategy would be to administer such compounds as lipophilic prodrugs, hypothesizing that such compounds would be slowly hydrolyzed to the active (carboxylate) form after absorption by *M. tuberculosis*. This strategy has successfully improved MIC values for anti-TB agents, with propyl ester prodrugs providing the most efficient *in vitro*

activities against *M. tuberculosis*.[38] Therefore, hybrid inhibitors in the form of propyl ester prodrugs might be expected to show activities against both the *Mtb*SDH enzyme and *M.* tuberculosis cells.

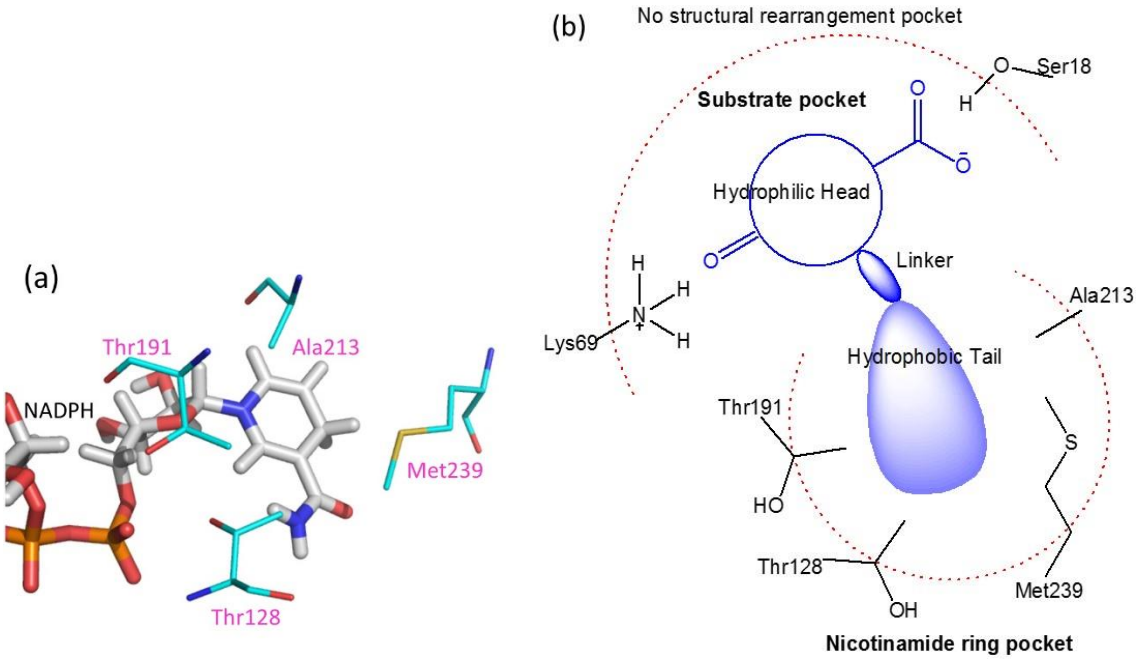

Figure 8. Rationale for hybrid *Mtb*SDH inhibitors. (a) Interactions of the NADPH nicotinamide ring in representative structure of the ternary *Mtb*SDH complex. **(b)** Proposed scaffold for hybrid inhibitors based on the binding of DHS substrate and NADPH nicotinamide ring as identified in simulations of the ternary DHS/NADPH/*Mtb*SDH complex.

CONCLUSIONS

Models of the binary DHS/*Mtb*SDH and ternary DHS/NADPH/*Mtb*SDH complexes, together with the apoenzyme, were generated and investigated using docking and MD simulations. Complexes of *Mtb*SDH mutants were also modelled to investigate the roles of Lys69 and Asp105 in binding and/or catalysis and the role of Ala213 in the stereospecific selection of the nicotinamide ring of NADPH. The results show that Lys69 plays a dual role, crucial for catalysis (proton transfer

to the C5 carbonyl of DHS) and for positioning the nicotinamide ring of NADPH for catalysis. Asp105 holds both the ε-amino group of Lys69 and the nicotinamide ring of NADPH in suitable positions to participate in the catalytic reaction of *Mtb*SDH. However, it made no contribution to DHS binding in the binary *Mtb*SDH complex. Furthermore, our work identifies the sidechain of Ala213 as the selection key for the *pro*S conformation of the NADPH nicotinamide ring of NADPH, differentiating *Mtb*SDH from related enzymes that instead utilize the *pro*R form. Finally, integration of the information obtained from this work provides three potential strategies for *Mtb*SDH inhibition, and allows us to propose the skeleton of a hybrid inhibitor able to utilize both the DHS and NADPH pockets to bind *Mtb*SDH. Future experiments will test this hypothesis.

ASSOCIATED CONTENT

Supporting Information. The total number of atoms in all systems for MD simulation, RMSD values of three backbone structures of *Mtb*SDH obtained from three MD simulations of all system, Cluster analysis of *Mtb*SDH systems, RMSD plots of all *Mtb*SDH systems, Flexibility of *Mtb*SDH, Rearrangement of *Mtb*SDH on DHS and SKM binding, Hydrogen bond analysis of DHS and NADPH binding in *Mtb*SDH complexes, Binding sites for the NADPH nicotinamide ring in *M. tuberculosis* and *H. pylori* SDH, The influence of K69A and D105N mutations on the decomposition energy of DHS in binary DHS/*Mtb*SDH complex

AUTHOR INFORMATION

Corresponding Author

*E-mail: auradee.punkvang@npu.ac.th

ACKNOWLEDGMENTS

This research was supported by the Thailand Research Fund (MRG5980152). Faculty of Science, Ubon Ratchathani University and the University of Bristol are gratefully acknowledged for

computational resource support of this research. We thank EPSRC for funding via BristolBridge (grant number EP/M027546/1) and CCP-BioSim (grant number EP/M022609/1).

REFERENCES

(1) World Health Organization (WHO). Global tuberculosis report 2017. http://www.who.int/tb/publications/global_report/en/ (accessed April 1, 2018).

(2) World Health Organization (WHO). Multidrug and Extensively Drug-Resistant TB (M/XDR-TB):2010 Global Report on Surveillance and Response. http://www.who.int/tb/features_archive/m_xdrtb_facts/en/ (accessed April 1, 2018).

(3) Velayati, A.A.; Farnia, P.; Masjedi, M.R.; Ibrahim, T.A.; Tabarsi, P.; Haroun, R.Z.; Kuan, H.O.; Ghanavi, J.; Farnia, P.; Varahram, M. Totally Drug-resistant Tuberculosis Strains: Evidence of Adaptation at the Cellular Level. *Eur. Respir. J.* **2009**, *34*, 1202-1203.

(4) Udwadia, Z.F.; Amale, R.A.; Ajbani, K.K.; Rodrigues, C. Totally Drug-resistant Tuberculosis in India. *Clin. Infect. Dis*. **2012**, *54*, 579-581.

(5) Roberts, F.; Roberts, C.W.; Johnson, J.J.; Kyle, D.E.; Krell, T.; Coggins, J.R.; Coombs, G.H.; Milhous, W.K.; Tzipori, S.; Ferguson, D.J.; Chakrabarti, D.; McLeod, R. Evidence for the Shikimate Pathway in Apicomplexan Parasites. *Nature* **1998**, *393*, 801-805.

(6) Keeling, P.J.; Palmer, J.D.; Donald, R.G.; Roos, D.S.; Waller, R.F.; McFadden, G.I. Shikimate Pathway in Apicomplexan Parasites. *Nature* **1999**, *397*, 219-220.

(7) Bentley, R. The Shikimate Pathway--A Metabolic Tree with Many Branches. *Crit. Rev. Biochem. Mol. Biol*. **1990**, *25*, 307-384.

(8) Ducati, R.G.; Basso, L.A.; Santos, D.S. Mycobacterial Shikimate Pathway Enzymes as Targets for Drug Design. *Curr. Drug Targets* **2007**, *8*, 423-435.

(9) Sassetti, C.M.; Boyd, D.H.; Rubin, E.J. Genes Required for Mycobacterial Growth Defined by High Density Mutagenesis. *Mol. Microbiol*. **2003**, *48*, 77-84.

(10) Dosselaere, F.; Vanderleyden, J. A Metabolic Node in Action: Chorismate-utilizing Enzymes in Microorganisms. *Crit. Rev. Microbiol*. **2001**, *27*, 75-131.

(11) Padyana, A.K.; Burley, S.K. Crystal Structure of Shikimate 5-dehydrogenase (SDH) Bound to NADP: Insights into Function and Evolution. *Structure* **2003**, *11*, 1005–10013

(12) Ye, S.; Von Delft, F.; Brooun, A.; Knuth, M.W.; Swanson, R.V.; McRee, D.E. The Crystal Structure of Shikimate Dehydrogenase (AroE) Reveals a Unique NADPH Binding Mode. *J. Bacteriol*. **2003**, *185*, 4144–4151.

(13) Michel, G.; Roszak, A.W.; Sauve, V.; Maclean, J.; Matte, A.; Coggins, J.R.; Cygler, M.; Lapthorn, A.J. Structures of Shikimate Dehydrogenase AroE and Its Paralog YdiB. A Common Structural Framework for Different Activities. *J. Biol. Chem*. **2003**, *278*, 19463–19472.

(14) Singh, S.; Korolev, S.; Koroleva, O.; Zarembinski, T.; Collart, F.; Joachimiak, A.; Christendat, D. Crystal Structure of a Novel Shikimate Dehydrogenase from *Haemophilus influenzae*. *J. Biol. Chem*. **2005**, *280*, 17101–17108.

(15) Peek, J.; Lee, J.; Hu, S.; Senisterra, G.; Christendat, D. Structural and Mechanistic Analysis of a Novel Class of Shikimate Dehydrogenases: Evidence for a Conserved Catalytic Mechanism in the Shikimate Dehydrogenase Family. *Biochemistry* **2011**, *50*, 8616–8627.

(16) Peek, J.; Garcia, C.; Lee, J.; Christendat, D. Insights into the Function of RifI2: Structural and Biochemical Investigation of a New Shikimate Dehydrogenase Family Protein. *Biochim. Biophys. Acta* **2013**, *1834*, 516–523.

(17) Fonseca, I.O.; Silva, R.G.; Fernandes, C.L.; de Souza, O.N.; Basso, L.A.; Santos, D.S. Kinetic and Chemical Mechanisms of Shikimate Dehydrogenase from *Mycobacterium tuberculosis*. *Arch. Biochem. Biophys.* **2007**, *457*, 123-133.

(18) Dansette, P.; Azerad, R. The Shikimate Pathway: II. Stereospecificity of Hydrogen Transfer Catalyzed by NADPH-dehydroshikimate Reductase of *E. coli*. *Biochimie* **1974**, *56*, 751-755.

(19) Bagautdinov, B.; Kunishima, N. Crystal Structures of Shikimate Dehydrogenase AroE from *Thermus thermophilus* HB8 and Its Cofactor and Substrate Complexes: Insights into the Enzymatic Mechanism. *J. Mol. Biol*. **2007**, *373*, 424-438.

(20) Rodrigues, V.S. Jr.; Breda, A.; Santos, D.S.; Basso, L.A. The Conserved Lysine69 Residue Plays a Catalytic Role in *Mycobacterium tuberculosis* Shikimate Dehydrogenase. *BMC Res Notes*. **2009**, *2*, 227.

(21) Singh, S.A.; Christendat, D. Structure of Arabidopsis dehydroquinate Dehydratase-Shikimate Dehydrogenase and Implications for Metabolic Channeling in the Shikimate Pathway. *Biochemistry* **2006**, *45*, 7787-7796.

(22) Morris, G.M.; Goodshell, D.S.; Halliday, R.S.; Huey, R.; Hart, W.E.; Belew, R.K.; Olson. A.J. Automated Docking using a Lamarckian Genetic Algorithm and Empirical Binding Free Energy Function. *J. Comput. Chem*. **1998**, *19*, 1639-1662.

(23) Case, D.A.; Betz, R.M.; Cerutti, D.S.; Cheatham, III, T.E.; Darden, T.A.; Duke, R.E.; Giese, T.J.; Gohlke, H.; Goetz, A.W.; Homeyer, N.; Izadi, S.; Janowski, P.; Kaus, J.; Kovalenko, A.; Lee, T.S.; LeGrand, S.; Li, P.; Lin, C.; Luchko, T.; Luo, R.; Madej, B.; Mermelstein, D.; Merz, K.M.; Monard, G.; Nguyen, H.; Nguyen, H.T.; Omelyan, I.; Onufriev, A., Roe, D.R.; Roitberg, A.; Sagui, C.; Simmerling, C.L.; Botello-Smith, W.M.; Swails, J.; Walker, R.C.; Wang, J.; Wolf, R.M.; Wu, X.; Xiao, L.; Kollman, P.A. AMBER 2016, University of California, San Francisco, CA, 2016.

(24) Pearlman, D.A.; Case, D.A.; Caldwell, J.W.; Ross, W.S.; Cheatham, III, T.E.; DeBolt, S.; Ferguson, D.; Seibel, G.; Kollman, P. AMBER, A Package of Computer Programs for Applying Molecular Mechanics, Normal Mode Analysis, Molecular Dynamics and Free Energy Calculations to Simulate the Structural and Energetic Properties of Molecules. *Comp. Phys. Commun*. **1995**, *91*, 1-41.

(25) Case, D.A.; Cheatham, T.; Darden, T.; Gohlke, H.; Luo, R.; Merz, K.M. Jr.; Onufriev, A.; Simmerling, C.; Wang, B.; Woods, R. The Amber Biomolecular Simulation Programs. *J. Comput. Chem*. **2005**, *26*,1668-1688.

(26) Wang, J.; Wolf, R.M.; Caldwell, J.W.; Kollman, P.A. Case, D.A. Development and Testing of A General Amber Force Field. *J. Comput. Chem*. **2004**, *25*, 1157-1174.

(27) Cieplak, P.; Cornell, W.D.; Bayly, C.; Kollman, P.A. Application of the Multimolecule and Multiconformational RESP Methodology to Biopolymers: Charge Derivation for DNA, RNA, and Proteins. *J. Comput. Chem*. **1995**, *16*, 1357-1377.

(28) Fox, T.; Kollman, P.A. Application of the RESP Methodology in the Parametrization of Organic Solvents. *J. Phys. Chem. B*. **1998**, *102*, 8070-8079.

(29) Bayly, C.I.; Cieplak, P.; Cornell, W.D.; Kollman, P.A. A Well-Behaved Electrostatic Potential Based Method Using Charge Restraints for Deriving Atomic Charges: The RESP Model. *J. Phys. Chem*. **1993**, *97*, 10269-10280.

(30) Jorgensen, W.L.; Chandrasekhar, J.; Madura, J.D.; Impey, R.W.; Klein, M.L. Comparison of Simple Potential Functions for Simulating Liquid Water. *J. Chem. Phys*. **1983**, *79*, 926-935.

(31) Darden, T.; York, D.; Pedersen, L.J. Particle Mesh Ewald-an NLog(N) method for Ewald sums in large systems. *J. Chem. Phys*. **1993**, *98*, 10089-10092.

(32) Ryckaert, J.P.; Ciccotti, G.; Berendsen, H.J.C. Numerical Integration of the Cartesian Equations of Motion of A System with Constraints: Molecular Dynamics of n-Alkanes. *J. Comput. Phys*. **1977**, *23*, 327-341.

(33) Roe, D. R.; Cheatham, T. III. PTRAJ and CPPTRAJ: Software for Processing and Analysis of Molecular Dynamics Trajectory Data. *J. Chem. Theory Comput*. **2013**, *9*, 3084–3095.

(34) Miller, B. R.; McGee, T. D.; Swails, J. M.; Homeyer, N.; Gohlke, H.; Roitberg, A. E. MMPBSA.py: An Efficient Program for End-State Free Energy Calculations. *J. Chem. Theory Comput*., **2012**, *8*, 3314–3321.

(35) Case, D.A.; Darden, T.A.; Cheatham, T.E., III; Simmerling, C.L.; Wang, J.; Duke, R.E.; Luo, R.; Walker, R.C.; Zhang, W.; Merz, K.M.; Roberts, B.; Hayik, S.; Roitberg, A.; Seabra, G.; Swails, J.; Götz, A.W.; Kolossváry, I.; Wong, K.F.; Paesani, F.; Vanicek, J.; Wolf, R.M.; Liu, J.;

Wu, X.; Brozell, S.R.; Steinbrecher, T.; Gohlke, H.; Cai, Q.; Ye, X.; Wang, J.; Hsieh, M.-J.; Cui, G.; Roe, D.R.; Mathews, D.H.; Seetin, M.G.; Salomon-Ferrer, R.; Sagui, C.; Babin, V.; Luchko, T.; Gusarov, S.; Kovalenko, A.; Kollman, P.A. AMBER 12, University of California, San Francisco, CA, 2012.

(36) Lavogina, D.; Enkvist, E.; Uri, A. Bisubstrate inhibitors of protein kinases: from principle to practical applications. *ChemMedChem*. **2010**, *5*, 23-34.

(37) Charman, W. N.; Porter, C. J. H. Lipophilic prodrugs designed for intestinal lymphatic transport. *Adv. Drug Delivery Rev.* **1996**, *19*, 149–169.

(38) Tizón, L.; Otero, J.M.; Prazeres, V.F.; Llamas-Saiz, A.L.; Fox, G.C.; van Raaij, M.J.; Lamb, H.; Hawkins, A.R.; Ainsa, J.A.; Castedo, L.; González-Bello, C. A Prodrug Approach for Improving Antituberculosis Activity of Potent *Mycobacterium tuberculosis* Type II Dehydroquinase Inhibitors. *J. Med. Chem*. **2011**, *54*, 6063-6084.

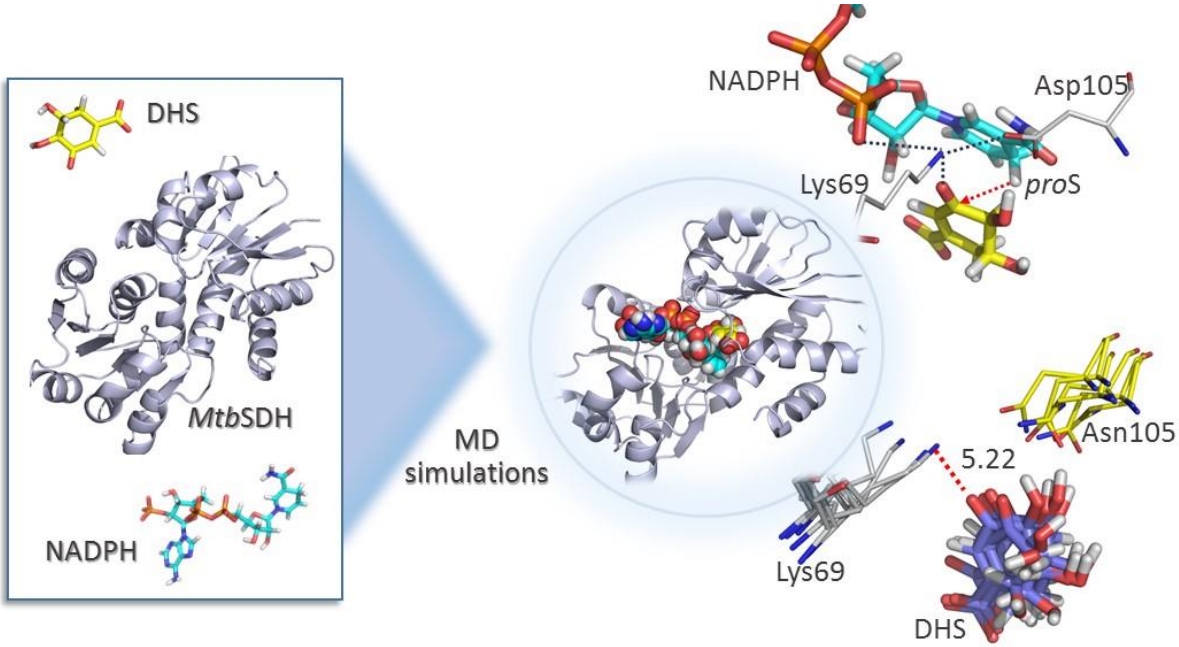

For Table of Contents Only